47th AIAA Aerospace Sciences Meeting Including The New Horizons Forum and Aerospace Exposition
5 - 8 January 2009, Orlando, Florida

AIAA 2009-904

47th AIAA Aerospace Sciences Meeting Including The New Horizons Forum and Aerospace Exposition, 5-8 Jan 2009, Orlando, Florida

Forebody Asymmetric Load Manipulated by a Horseshoe-Shaped Plasma Actuator

Jianlei Wang*, and Huaxing Li†
Northwestern Polytechnical University, Xi'an 710072, China
Feng Liu‡, Shijun Luo§
University of California, Irvine, CA 92697-3975

A pair of plasma actuators of horseshoe shape is proposed for dynamic manipulation of forebody aerodynamic load at high angles of attack. Preliminary wind tunnel pressure measurements show that asymmetric force over a conical forebody of semi-apex angle 10° can be manipulated by activating the plasma actuator mounted on one side of the cone tip. Further work is suggested.

Nomenclature

C_m	=	pitching-moment coefficient about cone base, pitching moment/$q_\infty SD$
C_N	=	overall normal-force coefficient, overall normal-force/$q_\infty S$
C_{Nd}	=	local normal-force coefficient, local normal-force/$q_\infty d$
C_n	=	yawing-moment coefficient about cone base, yawing moment/$q_\infty SD$
C_p	=	pressure coefficient
C_Y	=	overall side-force coefficient, overall side-force/$q_\infty S$
C_{Yd}	=	local side-force coefficient, local side-force/$q_\infty d$
D	=	base diameter of circular cone forebody
d	=	local diameter of circular cone forebody
F	=	frequency of a.c. voltage source
L	=	length of circular cone forebody
q_∞	=	free-stream dynamic pressure
Re	=	free-stream Reynolds number based on D
S	=	base area of circular cone forebody
U_∞	=	free-stream velocity
U_{max}	=	maximum velocity induced by plasma actuator in still air
V_{p-p}	=	peak-to-peak voltage of a.c. voltage source
w	=	input power
α	=	angle of attack
θ	=	meridian angle measured from windward generator, positive when clockwise

*Graduate Student, Department of Fluid Mechanics.
†Professor, College of Aeronautical Engineering.
‡Professor, Department of Mechanical and Aerospace Engineering. Associate Fellow AIAA.
§Researcher, Department of Mechanical and Aerospace Engineering.

I. Introduction

The most interesting phenomena associated with high angle of attack aerodynamics is the sudden onset of vortex asymmetry on the forebody of an air vehicle in symmetric flight. One of the first observations of vortex asymmetry onset was reported in 1951 by Allen and Perkins.[1] Interest in the phenomenon has been intensified since the late 1970's as concepts for highly maneuverable aircraft have been developed. These high-performance aircrafts are expected to operate routinely at high angles of attack at which vortex asymmetry is known to occur. When vortex asymmetry occurs, the aerodynamic, stability, and control characteristics of the vehicle change dramatically. In the mean time, the conventional aerodynamic controls become ineffective due to the vortex wakes generated by the forebody.

High-angle-of-attack flow control is most effective when applied at the region close with the point apex of the forebody. The presence of two closely-spaced vortices around the pointed forebody at high angles of attack enhances the effectiveness. Compared with the wing, control on the forebody is required over a much small area and thus physical requirements such as size and weight could be much smaller. The lengthy forebody of a modern fighter further enhances the control effectiveness by providing a long moment arm. Excellent reviews of this activity can be found in papers by Malcolm[2,3] and Williams.[4]

Hanff, Lee and Kind[5] used the duty cycle modulation of the alternating blowing from two forward facing nozzles to control the mean lateral aerodynamic forces and moments over slender bodies. The method takes the advantage of the inherently bi-stable nature of the forebody vortices by deliberately switching them between their two stable states.

Flow control with electromagnetic energy addition receives significant attention, since it is fully electronic with no mechanical parts and has a broard frequency bandwidth so that it can have fast response for feedback control. It is highly desirable to replace the blowing nozzles in the method of Hanff et al.[5] with a pair of plasma actuators of single dielectric barrier discharge (SDBD).[6] The present paper is aimed at the study of a plasma flow control over a pointed slender forebody of revolution.

Asymmetric vortices on slender body of revolution have been reported.[7] Hall[8] established an inherent relation between the vortex flow and the surface pressure distribution on a slender body by comparing oil flow visualization and surface pressure measurements in the literature. In the following sections, the experimental setup is described. The experinental results are then presented and discussed. Finally conclusions are drawn.

II. Experimental Setup

The tests are conducted in an open-circuit low-speed wind tunnel at the Northwestern Polytechnical University. The test section has a 3.0 $m \times 1.6$ m cross section. The model is rigidly mounted onto the support in the test section shown in Fig. 1. A thorough job of cleaning the model was done prior to each run of the wind tunnel.

Since the nose of any pointed forebody is locally conical in shape, the flow may be regarded as locally equivalent to that about a tangent cone. The basic features of the asymmetric flow can be displayed by studying the flows over a circular cone. The experimental model is a circular cone of 10° semi-apex angle faired to a cylindrical afterbody. The length of the cone is 463.8 mm and the cone base diameter is 163.6 mm. The cone tip of length 150 mm is made of plastic for plasma-actuator accommondation and the rest of the model is made of metal.

The SDBD plasma actuators are designed small and compact so that they can be placed as close with the cone apex as possible and without mutual interference. Three different designs of the actutors and mounting schemes have been tested.[9,10] The one studied in this paper is shown in Fig. 2. The plasma actuator consists of two copper electrodes of 0.03 mm thickness and a Kapton dielectric film to cover the encapsulated electrode from the exposed electrode. The shape of the exposed and encapsulated electrode is horseshoe and trapezoid, respectively, shown in Fig. 2. The length of the exposed electrode is 30 mm. The width of the exposed electrode is 1 mm. There is an including angle of 3° between the two legs of the horseshoe shown in Fig. 2(c). The encapsulated electrode lies between the exposed electrode legs. The leading-edge width of the encapsulated electrode is 2 mm. The two electrodes are separated by a gap of 1 mm, where the plasma is created. The effect of the SDBD actuator is to impart momentum to the flow like the forward facing nozzle used by Hanff et al.[5] but without the mass injection. The gap between the electrodes for our particular actuators was optimized for maximum induced air flow based on experiments

Figure 1. The model in the wind tunnel.

conducted in still air outside the wind tunnel.

A pair of the SDBD actuators are mounted on the cone surface symmetrically. The central lines of the actuators are located at the meridian angle $\theta \approx \pm 145^\circ$ shown in Fig. 2, where θ is measured from the windward generator and the positive is clockwise when looking upstream. The leading edge of the actuator is located at 20 mm from the cone apex. The plasma blows upward and forward along the meridian of the cone tip. The plasma-actuator arrangement is intended to push the tip vortex on the same side of the cone away from the cone surface. In the present study, the plasma actuators are made by hands and then attached to the cone tip surface with glue. No allowance is made on the cone surface for the attachment.

Two modes of operations of the actuators are defined. The plasma-off mode corresponds to the case when neither of the two actuators is activated. The port-on mode refers to the conditions when the port actuator is activated while the starboard actuator is kept off during the test. (The starboard-on mode is the conditions when the starboard actuator is activated while the port actuator is kept off, which is not studied in this paper.) Each of the two actuators on the cone model is separately driven by an a.c. voltage source (model CTP-2000K by Nanjing Suman Co.). The waveform of the a.c. source is sine wave. The peak-to-peak voltage is chosen based on a wind tunnel test shown in IIIB, $V_{p-p} = 12\ kV$ and frequency and $F = 8.9\ kHz$. The measured power consumption is approximately 15 W.

Figure 3 compares the smoke lines for the plasma off and the port plasma on in still air. The still-air experiments were conducted in a Plexiglas cover to shield the inside air from air flow within the laboratory. The air flow induced by the port plasma on is clearly shown in Fig. 3(b). The maximum speed of the induced flow on the plane perpendiculat to the cone axis at the apex, U_{max}, was measured with a hot-wire anemometer survey. Figure 4(a) shows the maximum speed, U_{max} vs. V_{p-p} at $F \approx 8.9\ kHz$.Fig. 4(b) gives the glow of the plasma flow in still air.

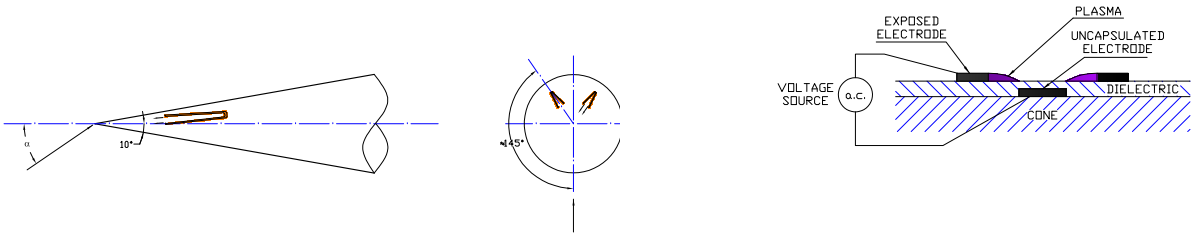

(a) arrangement (b) SDBD

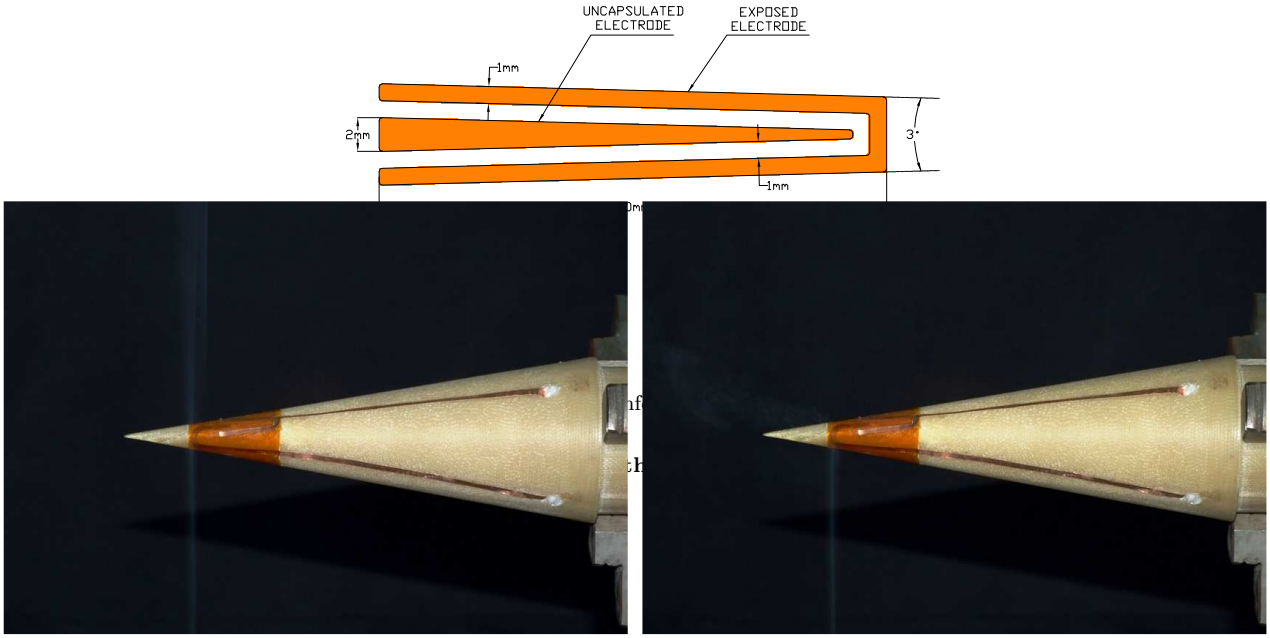

(a) plasma off (b) port plasma on

Figure 3. Comparison of smoke lines for plasma off and port plasma on in still air.

Surface pressure measurements are chosen for the model instrumentation to maximum the information provided about the complex flow and to allow much rigid mounting of the model required for the high-angle-of-attack tests. The 252 pressure tappings are arranged in rings of 36, every 10° around the circumference of the cone, at 7 stations uniformly distributed from $x/L = 0.340$ to 0.813 on the cone forebody. Details can be found in Ref. 11. Pressure reading from the transducers 9816 and 8400 made by the PSI Company are taken 64 and 127 times per second, respectively. The computer system was set up to output one- and five-second averages. A comparison of the measurements reveal that there are no differences in the one-second and five-second average pressures in our experiments. We present the five-second average data below. Among the total 252 pressure taps, fewer than 10 were found to give abnormal pressure readings, which are removed and replaced by linearly interpolated values from neighboring normal readings in the data processing phase.

III. Experimental Results and Discussions

In a typical bi-stable mode, the asymmetry may be either towards the starboard side or the port side, affected by slight imperfections of the cone near the apex and also free-stream conditions.[7] By taking advantage of the sensitivity of the flow on the conditions near the apex of the cone, we can control the vortex configuration and thus the pressure distribution asymmetry by activating one of the installed plasma

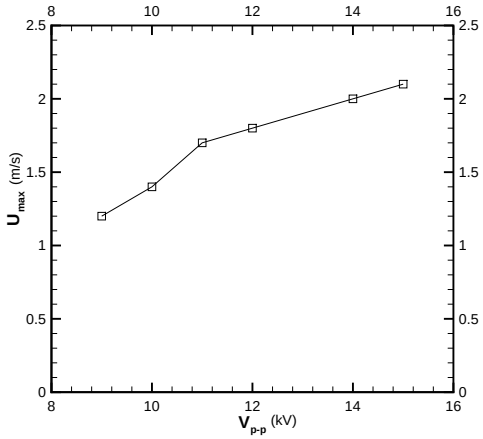

(a) maximum speed

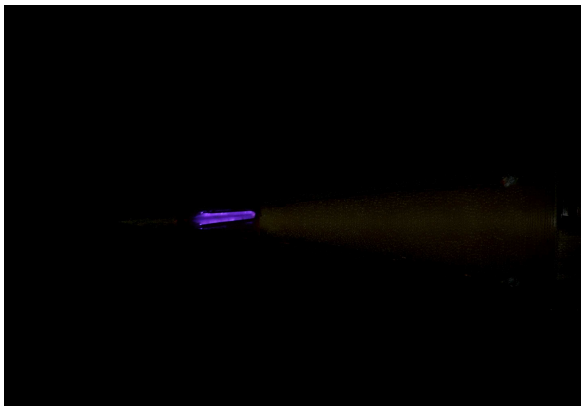

(b) plasma glow

Figure 4. Induced effects of port plasma actuation in still air.

actuators. Experiments were performed for the plasma-off and port-on. Two cases are presented: (1) $\alpha = 50^\circ$ and $U_\infty = 5\ m/s$, (2) $\alpha = 55^\circ$ and $U_\infty = 15\ m/s$. The corresponding Reynolds number based on the cone base diameter is 5×10^4 and 1.5×10^5, respectively. Starboard-on was not done, because the present plasma actuators are sensitive to the experimental setup. The actuator geometry is slender, a slight inaccuracies may lead to failure. Among the three different plasma actuators,[9,10] the horeshoe-shaped one requires the highest precision in model preparations. A refinement of the present model is required. Although the starboard-on is not done in the tests, a refined model would yield the hoped-for results for starboard-on, i.e., the mirror-imaged vortex pattern and the anti-symmetric pressure ditribution to the results of port-on, based on the intrinsic symmetry property.

A. Base Plasma-Off Flow at Zero Angle of Attack

In order to check the symmetry of the cone and model alignment in the wind tunnel, a test is run at zero angle of attack and with plasma off. The free stream velocity is set at $U_\infty = 5\ m/s$ and $15\ m/s$ in the present study. The corresponding Reynolds numbers based on the cone base diameter are 5×10^4 and 1.5×10^5. Fig. 5 presents the pressure distributions at plasma off, $U_\infty = 5\ m/s$ and $15\ m/s$, and $\alpha = 0^\circ$. Aside from some slight irregularities, the measured pressure distributions indicate essentially an axisymmetric flow around the cone. In the present study, the hand-made plasma actuators and no allowance for the attachment could have been the cause for the mentioned irregularities of the pressure distributions. Nevertheless, the disturbances were tolerably small.

B. Choice of Peak-to-Peak Voltage on Wind-Tunnel Test Results

The choice of the peak-peak voltgage is based on a study of measured pressures. Fig. 6 compares the pressure distributions for different peak-to-peak voltages of the port plasma actuator at $F \approx 8.9\ kHz$, $\alpha = 50^\circ$, $U_\infty = 5\ m/s$, Stations 1 and 7. As the peak-to-peak voltage is increased to $12\ kV$, the pressure distribution approaches a limit. Thus, $V_{p-p} = 12\ kV$ is chosen. In Fig. 6 the plasma-off pressure distributions are attached for reference.

The forces and moments acting on the cone forebody are calculated from the measured pressures by assuming that the pressure distributions are conical over each segment along the cone length which is divided by the mid points of the neighboring stations. The local forces are normalized with the local diameter of the cone. Figure 7 presents the local side- and normal-force acting on the cone forebody versus x/L for different peak-to-peak voltages of the port actuator at $F \approx 8.9\ kHz$, $\alpha = 50^\circ$, $U_\infty = 5\ m/s$. The results confirm that $V_{p-p} = 12\ kV$ is a good choice.

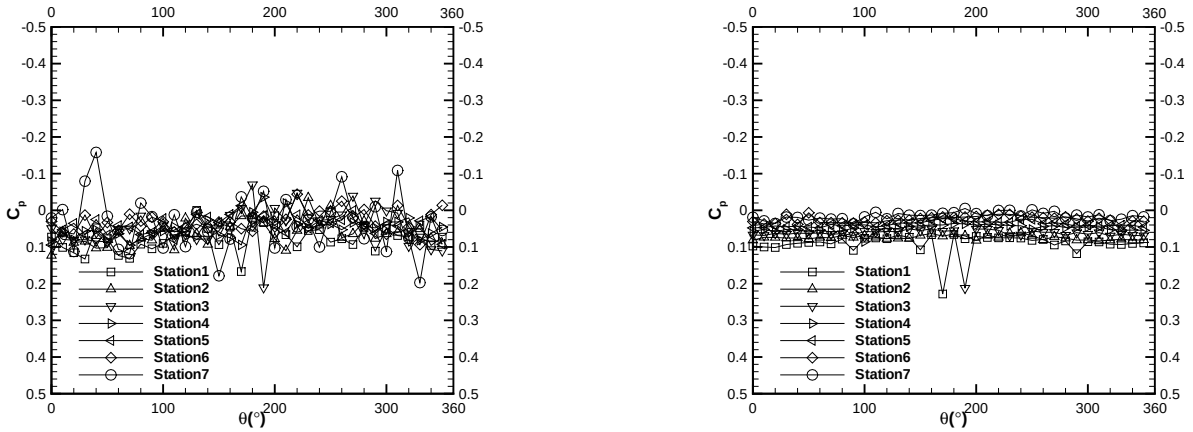

(a) $U_\infty = 5\ m/s$ (b) $U_\infty = 15\ m/s$

Figure 5. Comparison of pressure distributions at plasma off, $U_\infty = 5\ m/s$ and $15\ m/s$, and $\alpha = 0°$.

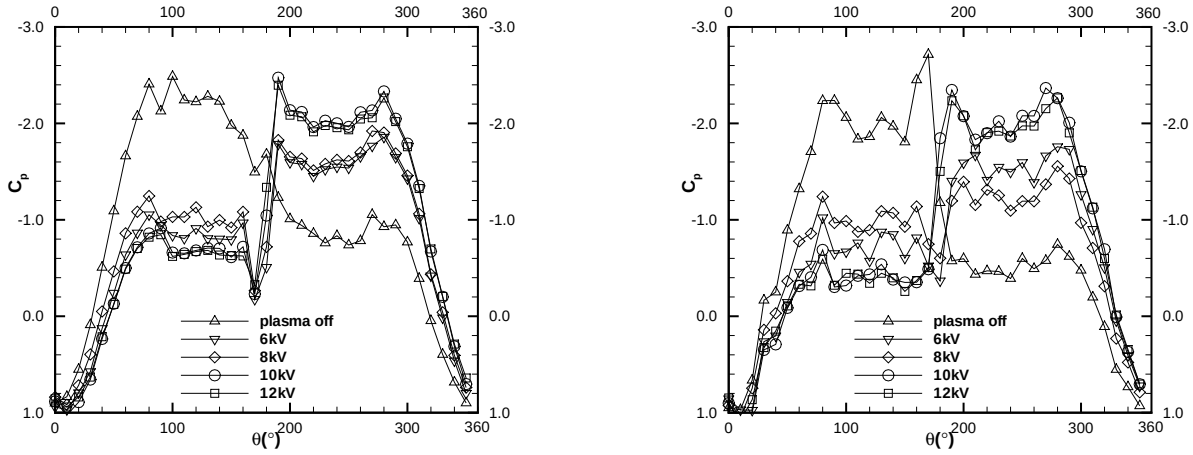

(a) station 1 (b) station 7

Figure 6. Comparison of pressure distributions for different peak-to-peak voltages of port plasma actuator at $F \approx 8.9\ kHz$, $\alpha = 50°$, $U_\infty = 5\ m/s$.

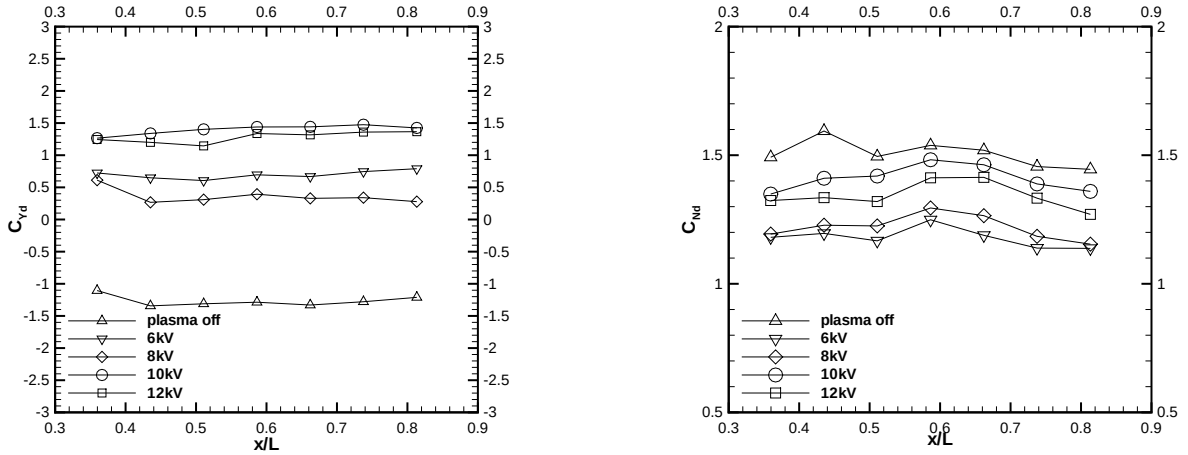

(a) local side force

(b) local normal force

Figure 7. Comparison of local side- and normal-force vs. x/L for different peak-to-peak voltages of the port actuator at $F \approx 8.9\ kHz$, $\alpha = 50°$, $U_\infty = 5\ m/s$.

The overall forces and moments are then calculated from the measured pressures and normalized with the area and diameter of the cone base. The moments are taken about the cone base. The yawing moment is positive when yawing to the starboard side of the cone. Fig. 8 gives the overall side-force and yawing-moment coefficients vs. peak-to-peak voltage of the port actuator at $F \approx 8.9\ kHz$, $\alpha = 50°$, $U_\infty = 5\ m/s$. Fig. 8 shows that $C_Y \approx -2.2$ and 2.4 at $V_{p-p} = 0\ kV$ and $12\ kV$, respectively, and similar results occur for C_n, which indicates that the port plasma actuated at $V_{p-p} = 12\ kV$ induces the mirror image asymmetric flow with respect to that of plasma off. Hence $V_{p-p} \approx 12\ kV$ with $F \approx 8.9\ kHz$ is used in the following.

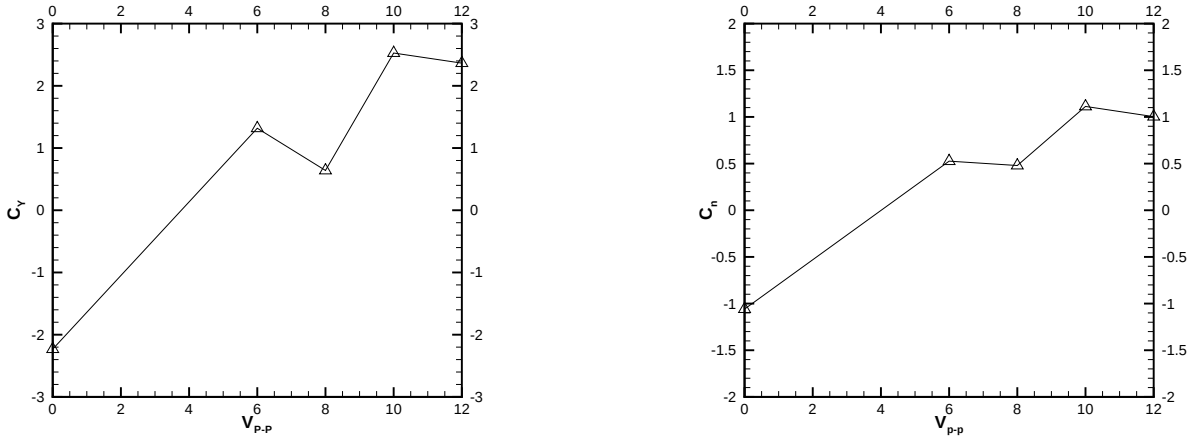

(a) overall side force

(b) yawing moment

Figure 8. Overall side-force and yawing-moment coefficients vs. peak-to-peak voltage of the port actuator at $F \approx 8.9\ kHz$, $\alpha = 50°$, $U_\infty = 5\ m/s$.

C. Comparison of Plasma-Off and Port-On Results, $\alpha = 50°$

Figure 9 compares the pressure distributions for the plasma off and port on at $\alpha = 50°$, $U_\infty = 5\ m/s$, Stations 1 and 7. The plasma-off pressure ditributions in Fig. 9 show a stronger suction on the port side than that

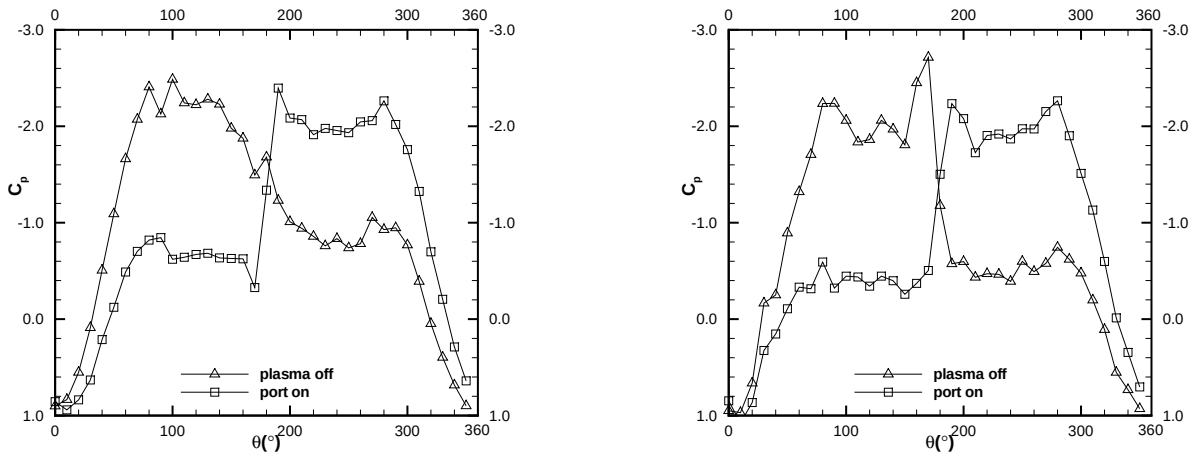

(a) station 1

(b) station 7

Figure 9. Comparison of pressure distributions for plasma off and port plasma on at $\alpha = 50°$, $U_\infty = 5\ m/s$.

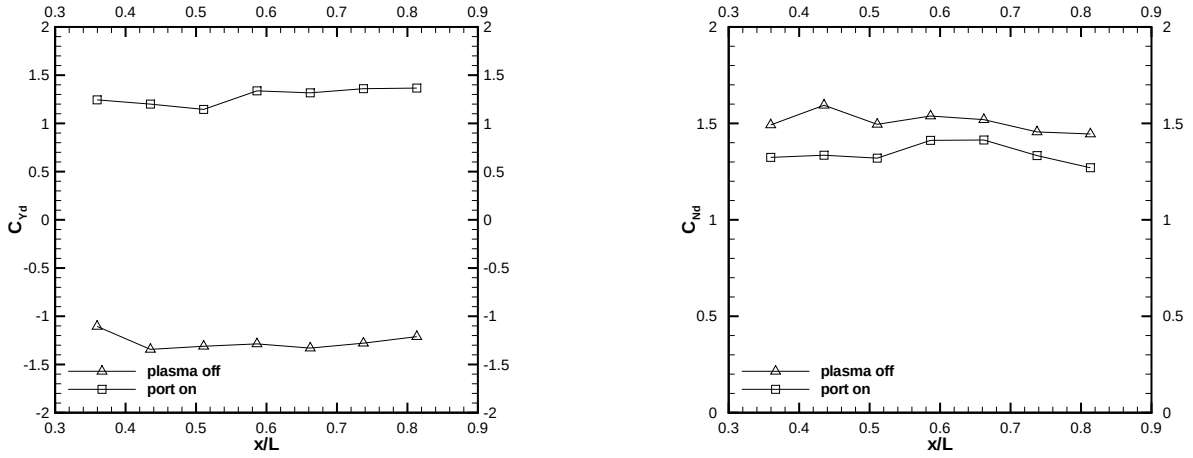

(a) local side force

(b) local normal force

Figure 10. Local side- and normal-force vs. x/L at $\alpha = 50°$, $U_\infty = 5\ m/s$.

on the starboard side of the cone, indicating that the port-side vortex is located closer with the cone than the starboard-side vortex.[8] The port-on pressure distributions show stronger suction on the starboard side of the cone, indicating that the starboard-side vortex has moved close to the cone while the port-side vortex moved away from the cone. The port plasma actuator induces a momentum input in forward and upward directions, which presumably pushes the port-side vortex away from the cone surface and in the mean time brings the starboard vortex with its feeding shear-layer close by the cone. Similar effects were observed by Hanff, et al.[5] Flow visualizations to reveal the detailed mechanism are suggested.

Figure 10 presents the local side- and normal-force along the cone axis at $\alpha = 50°$, $U_\infty = 5\ m/s$. The local side- and normal-forces shown in Fig. 10 are nearly constant for each mode, indicating the cross-flow pattern remains the same along the cone axis for each mode. The plasma-off local side forces are negative. The port-on local side forces switch to positive, confirming that the stronger suctions switch to the starboard side seen in Fig. 9. The local normal forces remain positive and almost constant along the cone axis, and nearly equal for plasma off and on, and have the same order of magnitudes of the local side forces.

D. Comparison of Plasma-Off and Port-On Results, $\alpha = 55°$

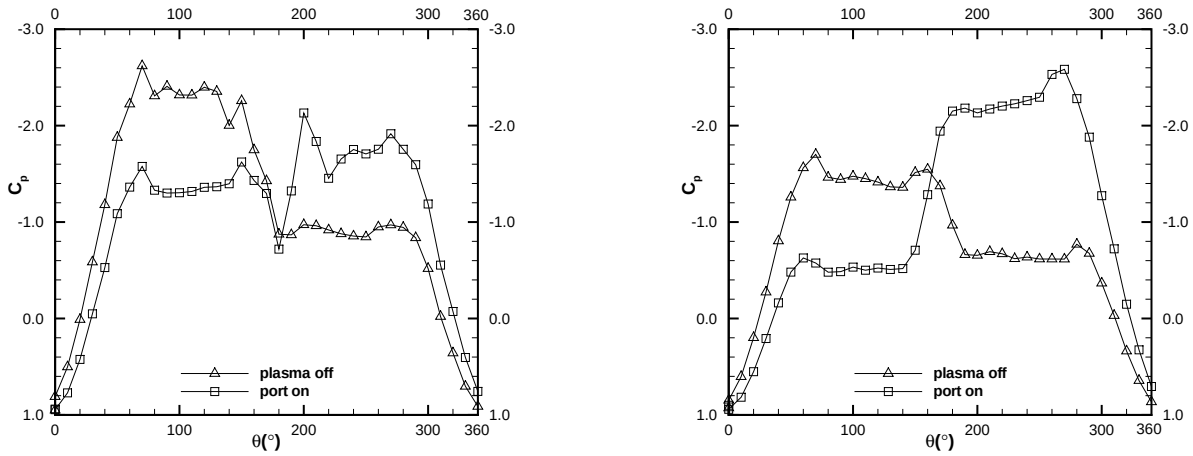

(a) Station 1

(b) Station 7

Figure 11. Comparison of pressure distributions for the plasma off and port plasma on at $\alpha = 55°$, $U_\infty = 15\ m/s$.

The pressure distributions for the plasma off and port plasma on are compared at $\alpha = 55°$, $U_\infty = 15\ m/s$, and Stations 1 and 7 in Fig. 11. Like Fig. 9, the stronger sunction of the pressure distributions for plasma off is located on the port side of the cone and that for the port on is switched to the starboard side. The mechanism of the plasma actuation in this case is the same as stated in the previous case. Fig. 12 presents the local side- and normal-force acting on the cone forebody versus x/L at $\alpha = 55°$, $U_\infty = 15\ m/s$. In this case the local side- and normal-force along the cone axis do not remain nearly unchanged anymore. For port on, C_{Yd} in the front region is significantly lower than that behind. For plasma off the C_{Yd} magnitude varies in opposite direction and the change is not so significant. The variations indicate that the cross-flow patterns at $\alpha = 55°$ for port on and plasma off along the cone axis are different from those at $\alpha = 50°$ shown in Fig. 10. The port-on is effective when the freestream velocity is as large as 15 m/s ($Re = 1.5 \times 10^6$), which favors applications of plasma flow control.

E. Comparison of Pressure Distributions over All Stations

To explain the different local force variations memtioned above, the detail pressure data are studied here. Figs. 13 and 14 present the pressure distributions over all stations of the cone for $\alpha = 50°$, $U_\infty = 5\ m/s$ and $\alpha = 55°$, $U_\infty = 15\ m/s$, respectively. In the former case all the pressure distributions nearly overlap for plasma off and port on. In the later case the pressure distributions varies drastically along the cone axis.

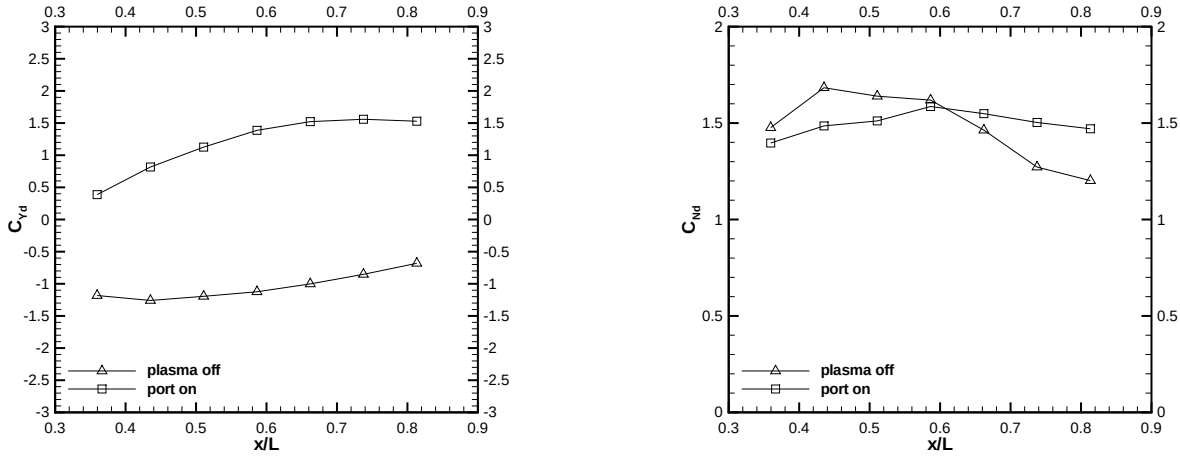

(a) local side force

(b) local normal force

Figure 12. Local side- and normal-force vs. x/L at $\alpha = 55°$, $U_\infty = 15\ m/s$.

Fig. 14(b) shows the suction difference between the two sides of the cone is significantly lowered at Station 1. .

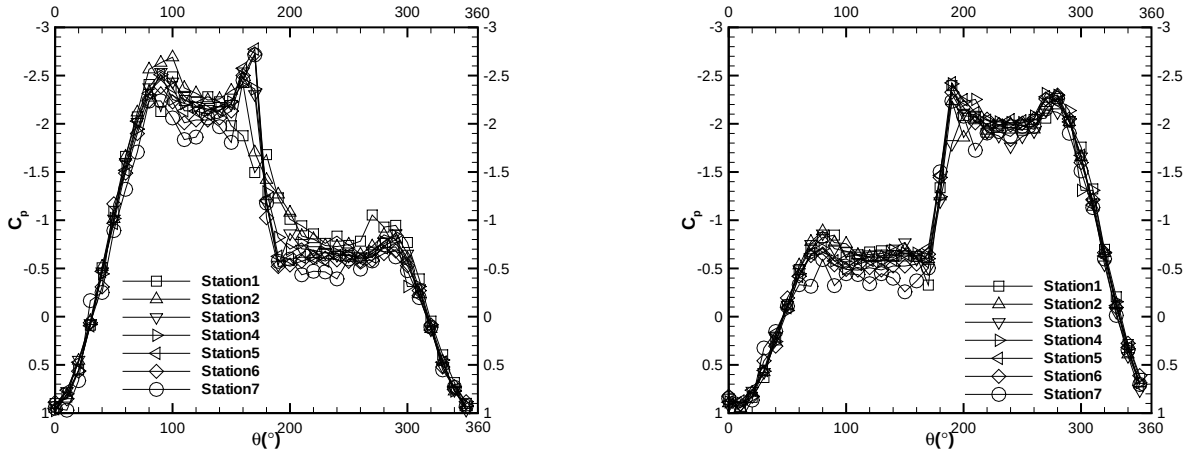

(a) plasma off

(b) port on

Figure 13. Comparison of pressure distributions over all stations for the plasma off and port plasma on at $\alpha = 50°$, $U_\infty = 5\ m/s$.

F. Comparison of Overall Forces and Moment Results

Table 1 compares the overall force- and moment-coefficients for the two modes. For the case of $\alpha = 55°$, the port-on yawing moment has a magnitude significantly lower than that for plasma off, while the port-on and plasma-off side forces have almost equal magnitudes. This is due to the moment arm effect in the yawing-momont calculations. The overall side force for port-on remains positive large value at $\alpha = 55°$ as that at $\alpha = 50°$, which differs from Liu et al.[9] and the reason is unclear. Besides, the free stream velocity is as large as 15 m/s at $\alpha = 55°$. Supposing that the starboard-on would be as effective as the port-on, the upper limit of duty cycled plasma control[9] could be increased to greater than 55°.

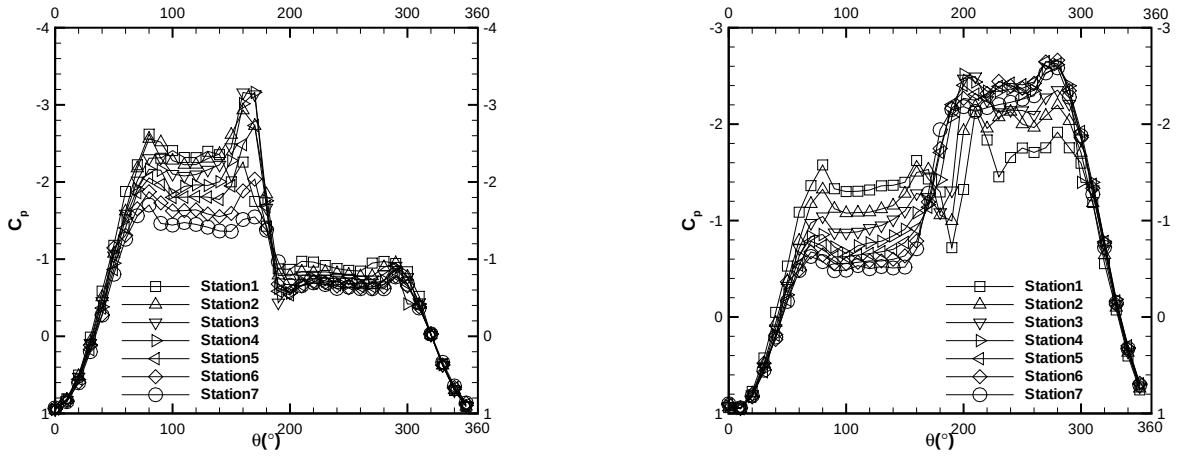

(a) plasma off

(b) port on

Figure 14. Comparison of pressure distributions over all stations for the plasma off and port plasma on at $\alpha = 55°$, $U_\infty = 15\ m/s$.

Table 1. Comparison of overall forces and moments for plasma off and port plasma on.

		C_Y		C_n		C_N		C_m	
α	U_∞	plasma off	port on	plasma off	port on	plasma off	port on	plasma off	port on
50°	$5\ m/s$	−2.2	2.4	−1.1	1.0	2.7	2.4	1.3	1.2
55°	$15\ m/s$	−1.7	2.3	−1.3	0.4	2.7	2.7	1.5	1.3

IV. Conclusions

Two horseshoe-shaped plasma actuators are symmetrically mounted on the leeward side of a conical forebody near the apex for dynamic manipulation of forebody lateral loads at high angles of attack.The plasma actuators are small and compact so that the two actuators can be placed extremely close with the forebody apex and without mutual interference. The plasma blows forward and upward over the leeward surface of the conical forebody toward the same-side tip vortex from behind and below to push it away from the body. Although the present investigations are restricted to the activation of the port-side actuator, they clearly demonatrate that by appropriately designing plasma actuators and chosing electric parameters, it is possible to obtain a bi-stable asymmetric loads at high angles of attack which is a highly desirable characteristics for proportional control of asymmetric loads.

Further investigations should be pursued to refine the model and complete the test with the starboard-side actuator.

Acknowledgment

The present work is supported by the Foundation for Fundamental Research of the Northwestern Polytechnical University, NPU-FFR-W018101.

References

[1]Allen, H. J. and Perkins, E. W., "A study of the effects of viscosity on the flow over slender inclined bodies of revolution," NACA TR 1048, 1951.

[2]Malcolm, G., "Forebody vortex control," *Prog. Aerospace Sci.*, Vol. 28, 1991, pp. 171–234.

[3]Malcolm, G., "Forebody vortex control–a progress review," AIAA Paper 93-3540, Aug. 1993.

[4]Williams, D., "A review of forebody vortex control scenarios," AIAA Paper 97-1967, June 1997.

[5]Hanff, E., Lee, R., and Kind,R.J., "Investigations on a dynamic forebody flow control system," Proceedings of the IEEE Conference, 1999, 99-0-7803-5715-9, pp. 28.1–28.9.

[6]Post, M., "Plasma actuators for separation control on stationary and oscillating airfoils," Ph.D Dissertation, University of Notre Dame, 2004.

[7]Zilliac, G. G., Degani, D., and Tobak, M., "Asymmetric vortices on a slender body of revolution," *AIAA Journal*, Vol. 29, No. 5, May 1991, pp. 667–675.

[8]Hall, R.M., "Influence of Reynolds number on forebody side forces for 3.5-diameter tangent-ogive bodies," AIAA-87-2274, Jun. 1987

[9]Liu, F., Luo, S.J.,Gao, C., Meng, X.S., Hao, J.N., Wang, J.L. and Zhao, Z.J., "Duty Cycle Plasma Flow Control over a Circular Cone Forebody," AIAA-2009-1082, Jan. 2009.

[10]Zhao, Z.J., Li, H.X., Liu, F. and Luo, S.J., "Forward-Blowing Plasma Actuation over Forebody Asymmetric Vortex," AIAA-2009-0752, Jan. 2009.

[11]Meng, S. , Qiao, Z., Gao, C., Luo, S., and Liu, F, "Reynolds number effects on cone forebody side force," AIAA Paper 2008-4303, June 2008.